Transactions of the **14th International Conference on Structural Mechanics in Reactor Technology** (SMiRT 14), Lyon, France, August 17-22, 1997 **G12/3**

Study on the fracture behavior of bi-material made of A508 steel and incoloy 825

Kikuchi M., Sasamoto H.
Science University of Tokyo, Japan

Abstract

The bi-material, where the Incoloy 825 is cladded on A508 steel, is used for the fracture test. The effect of the phase boundary on the fracture process is studied. Through cracked specimen and semi-circular cracked specimens are tested by the three point bending. The fatigue crack shape and the stable crack growth amount along the crack front are measured and the effect of the phase boundary is discussed. The precise FEM(Finite Element Method) analyses are conducted and the crack tip stress field is discussed.

1 Introduction

The effect of the phase boundary of bi-materials on the fracture behavior is one of the most important problem in the nuclear plant. In the elastic case, it is well known that the singular stress field exists at the phase boundary, and the characteristics of the singularities have been studied well. In the elastic-plastic case, the problem becomes more complicated because the number of parameters affecting fracture behavior is much larger than for the homogeneous material. In the homogeneous material, J integral is used as the fracture parameter in the elastic-plastic field[1,2]. But recently it has been pointed out that the J is not an unique controlling parameter at the crack tip. O'Dowd and Shih[3,4] proposed J-Q method instead of J integral method. In the inhomogeneous problem, it is pointed out that the Q factor plays an important role in the ductile fracture process[5].

In Japan, the EPI(Elastic-Plastic fracture mechanics of Inhomogeneous material) project was organized by Prof. Yagawa during 1988-1994, and more than 30 researchers have worked together on the EPI problem. The results of this study were published in Nuclear Engineering Design as the special volume[6].

This paper provides further results of this EPI project. New bi-material is made by cladding the Incoloy 825 on A508 steel. Several kinds of cracks are introduced near the phase boundary of this bi-material, and the fatigue test and the ductile fracture test are conducted. The effect of the phase boundary on the crack growth behavior is studied. After the test, the crack growth simulation is conducted by the three- and two-dimensional FEM analyses. The crack tip singular fields are obtained and their effects

on the crack growth behavior are discussed.

2 Test Specimen

The bi-material plate is made by the cladding Incoloy 825 on A508 steel, which is the steel for the reactor pressure vessel. By the ultra-sonic scanning, it is shown there is no initial defects in the phase boundary. The mechanical properties of both steels are shown in Table 1. The yield stress of A508 steel is much larger than that of Incoloy 825. The stress-strain relations of both metals are approximated by the following equations.

$$\epsilon = \frac{\sigma}{E} \qquad \text{for } \sigma \leq \sigma_y \tag{2.1}$$

$$\epsilon = \frac{\sigma}{E} + \left\{ \left(\frac{\sigma}{E}\right)^n - \left(\frac{\sigma_y}{E'}\right)^n \right\} \qquad \text{for } \sigma \geq \sigma_y \tag{2.2}$$

where σ_y is the yield stress, E is Young's modulus, and $E' = 900MPA$, $n = 10$ for A508 steel and $E' = 880MPa$, $n = 5$ for Incoloy 825.

Both equations are approximated by the Ramberg-Osgood type equation as

$$\frac{\epsilon}{\epsilon_y} = \frac{\sigma}{\sigma_y} + \alpha \left(\frac{\sigma}{\sigma_y}\right)^n \tag{2.3}$$

For A508 steel, $\alpha = 4$ and $n = 10$, and $\alpha = 4$ and $n = 6$ for Incoloy 825.

Two kinds of through cracked specimens and two surface cracked specimens are made for the fracture test. Figure 1 shows IA-T(Incoloy-A508 Through crack) specimen. The initial crack is introduced in Incoloy 825 steel by fatigue, and the crack tip exists in Incoloy side. The distance between the crack tip and the phase boundary is changed in 3 cases from 1.65mm to 0.2mm. Figure 2 is the AI-T(A508-Incoloy Through crack) specimen, where the initial crack exists in A508 steel and grows to the phase boundary. The distance between the crack tip and phase boundary is changed in 3 cases from 1.5mm to 0.3mm. Figure 3 shows surface cracked specimens. The shape of the surface crack is semi-elliptical and the aspect ratio of the crack is 1/3. The surface crack is introduced by EDM(Electric Discharge Machining), and the fatigue crack is not introduced. In IA-S1 specimen, Figure 3(a), the surface crack tip exists in the Incoloy 825 steel, and in IA-S2 specimen, Figure 3(b), the surface crack crosses with the phase boundary near the bottom of the crack. The stable crack growth tests are conducted by the three point bending test. After the test, the specimen is broken by fatigue, and the fracture surface is observed by SEM(Scanning Electron Microscope).

3 Experimental Results

Figure 4 shows the fracture surface of IA-T specimen. The fatigue crack is the deepest at the center of the specimen, which agrees with the result of the homogeneous specimen. The stable crack grows to the phase boundary, and the debonding occurs at the phase boundary. Then the stable crack does not exceed the phase boundary. The result of AI-T specimen shows different fracture process. The fatigue crack length becomes the maximum at the free surface. This is different from the result of homogeneous specimen. This is the effect of the phase boundary. The stable crack grows forward and does not

terminate at the phase boundary. It exceeds the phase boundary and grows into the Incoloy 825. The effect of the phase boundary on the ductile fracture process appears clearly.

The distributions of the stable crack growth amount, Δa, of IA-S1 specimen are shown in Figure 5. The abscissa is the deviatric angle which shows the location on the surface crack front normalized by $\pi/2$. $2\Phi/\pi = 0$ means the free surface, and the crack bottom is expressed by 1.0. Δa increases gradually due to the increase of Φ, until $2\Phi/\pi = 0.7$. Over this value, Δa begins to decrease. Over $2\Phi/\pi = 0.7$ area, the growing crack reaches to the phase boundary and terminates here. The debonding of two materials along the interface occurs.

The fracture surface of the AI-S2 specimen is shown in Figure 6. This is the photo near the phase boundary. Near the phase boundary, the Δa reaches to the boundary, but it does not exceeds the boundary. In A508 steel side, small amount of crack growth is observed. The distributions of Δa of this specimen along the crack front is shown in Figure 7. Δa at the phase boundary in Incoloy 825 shows special large value, but in other location, it shows similar value.

Through these experiments, the effect of the phase boundary is recognized in the following two points. (i) On the fatigue crack growth from A508 steel to Incoloy 825. (ii) The stable crack growth terminates when the crack grows from Incoloy to A508. But it exceeds the boundary when the crack grows from A508 to Incoloy 825. These effects are related with the difference of yield stress between two metals. By ref[7], the effect of the Young's modulus on the crack growth behavior in bi-material is discussed. In this case, the Young's Modulus of both materials are considered to be nearly same. But the difference of the yield stress affects on the crack growth behavior in the similar manner. It is also related with the difference of the crack tip stress fields from the HRR fields. It is studied by FEM analysis.

4 FEM Analysis

4.1 Fatigue crack growth analysis

Figure 8 shows the FEM model of AI-T specimen. To simulate the fatigue crack growth, the initial crack front shape is assumed to be the straight line, which is made by metal saw. By the elastic analysis, the distribution of the stress intensity factor, K_I, along the crack front is obtained. It is assumed that the fatigue crack growth occurs where the K_I is the maximum. Then the elastic analysis is repeated for the new crack front shape. This process is repeated until the distribution of K_I becomes nearly equal along the crack front. The final result of IA-T specimen is shown in Figure 9. The abscissa is the thickness direction normalized by the specimen thickness, t. $b/t = 0.0$ is the center of the crack front. In this figure, it is shown that the K_I distribution is nearly equal along the crack front, and the crack length becomes the maximum at the center of the plate. This results agree well with the experimental observation.

Figure 10 is the results of AI-T specimen. In this case, the crack grows from upward to downward in this figure. The crack length becomes the maximum at the free surface of the specimen, which also agrees with the experiment well. It became obvious that the stress intensity factor is the dominant parameter for the fatigue crack growth in the bi-material over the phase boundary.

4.2 Elastic-plastic analysis

The J integral is evaluated in the elastic-plastic analysis. Figure 11 is the results of two dimensional analysis of IA-T specimen. By changing the crack length, the J value for the constant load $P = 11.8N$ is calculated. The abscissa is the crack length. When $a/W = 0.4$, the crack front crosses the phase boundary. The J value increases gradually in the Incoloy 825 due to the increase of the crack length. But over the boundary, the J value terminates, it does not increase largely in A508 steel. Figure 12 is the similar result of AI-T specimen, where the applied load is kept to $P = 49N$. In this case, the J integral keeps to increase over the phase boundary. They are related with the crack growth behavior near the phase boundary.

Figure 13 shows the three dimensional FEM model of IA-S1 specimen. The distribution pattern of the J integral is shown in Figure 14. The J value is the minimum near the free surface, and increase gradually inside of the specimen. Over $2\Phi/\pi = 0.7$, the J value becomes nearly constant. This is different from those of homogeneous specimen. As shown in the author's previous paper[8], the J integral becomes the maximum where $2\Phi/\pi$ is about 0.7 or 0.8. The result of Figure 14 means that the J value distribution is affected by the existence of the phase boundary.

Figure 15 is the J distribution of IA-S2 specimen. The J value is nearly equal along the crack front in the Incoloy 825, an it increases a little in A508 steel. In the experiment, the stable crack growth becomes the maximum at the phase boundary, which is different from the J distribution pattern. In the author's previous paper[8], it is shown that the Q factor plays an important role in the ductile fracture process near the phase boundary. The Q factor distribution along the crack front in this specimen is shown in Figure 16. The Q factors decrease suddenly near the phase boundary in the Incoloy 825, which is not related with the behavior of Δa. It is difficult to estimate the stable crack growth behavior by the J-Q parameters.

4.3 Fracture Simulation by Void Growth Analysis

By the SEM(Scanning Electron Microscope) observation, it is shown that the dimple fracture is the main fracture process of both materials. Then the fracture simulation considering the void nucleation, growth and coalescence during the dimple fracture is conducted using Gurson's constitutive equation. The critical void volume fraction is determined by measuring the number and diameter of dimples in the fracture surface as $f_F = 0.22$ for A508 and 0.28 in Incoloy 825. Two dimensional plane-strain analysis are conducted based on the finite deformation theory. The mesh pattern of IA-T model is shown in Figure 17. Near the crack tip, very fine mesh is used.

Figure 18 shows the fracture process of IA-T specimen. The left side is the Incoloy 825, and the initial crack exists here. The left side is the A508 steel. The black area means that the fracture occurs in these elements. The fracture area spreads upward in Incoloy 825, and does not grow into A508. In A508 steel, there is no fracture area after some amount of crack growth. In Figure 19, the results of AI-T specimen are shown. The fracture area spread from the initial crack tip to the phase boundary. It exceeds the phase boundary, and the fracture area spreads to the Incoloy 825 steel. These results agree with the experimental results qualitatively. It is shown that the effect of the phase boundary is evaluated by using the Gurson's method in the simulation of the dimple fracture process even for the inhomogeneous material.

5 Conclusion

Using the bi-material specimen, the fatigue and dimple fracture tests are conducted, and the results are discussed with the results of FEM analysis. Following results are obtained.
(1) The fatigue crack growth behavior is affected by the existance of the phase boundary, but it is controlled by the stress intensity factor.
(2) The ductile fracture is largely affected by the phase boundary. The J integral is not an unique parameter for this problem.
(3) The fracture simulation using Gurson's model is conducted and the results agree with experiments qualitatively.

References

1. J.W. Hutchinson, J. Mech. Phys. Solids, 16(1968), pp.13-31.
2. J.R. Rice and G.F. Rosengren, Ibid 16(1968), pp.1-12
3. N.P. O'Dowd and C.F. Shih, J. Mech. Phys. Solids, 39(1991), p.989
4. N.P. O'Dowd and C.F. Shih, Ibid, 40(1992), p.939
5. M. Kikuchi, Int. J. Pres. Ves. & Piping, 63(1995), pp.315-326
6. Int. J. Pres. Ves. & Piping, 63 (1995)
7. H. Miyamoto and M. Kikuchi, Numerical Methods in Fracture Mechanics, Pineridge Press (1980), p.359
8. M. Kikuchi, Int. J. Fracture, 58(1992), pp.273-283

Table 1 Mechanical properties.

Material	Young's Modules[GPa]	Yield Stress[MPa]	Poisson's Ratio
A508 Steel	206	570	0.3
Incoloy825	182	380	0.3

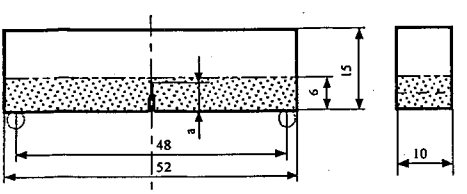

Fig.1 IA-T(Incoloy825 to A508 steel-Through crack) specimen.

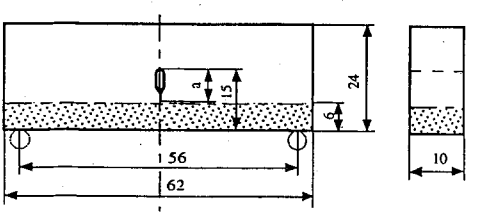

Fig.2 IA-T(A508 steel to Incoloy825-Through crack) specimen.

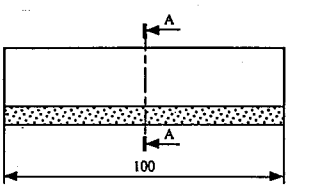

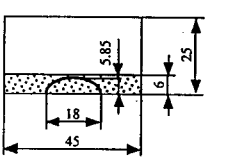

(a) IA-S1 specimen

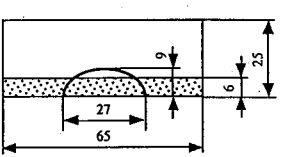

(b) IA-S2 specimen

Fig.3 Surface cracked specimens.

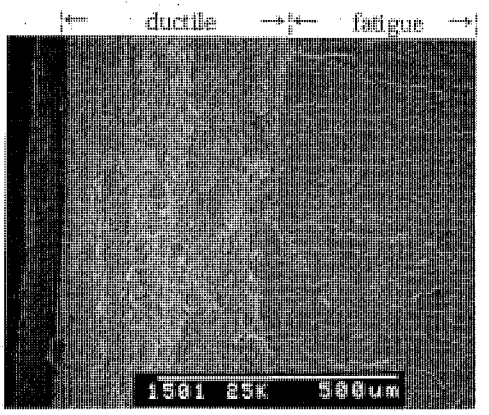

Fig.4 Fracture surface of IA-T specimen near the phase boundary.

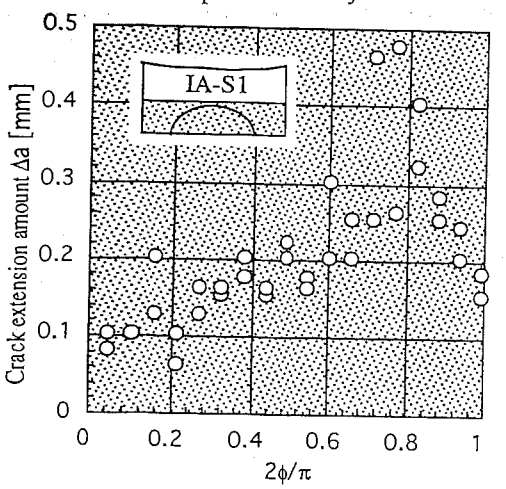

Fig.5 Stable crack growth amount △a of IA-S1 specimen along the crack front.

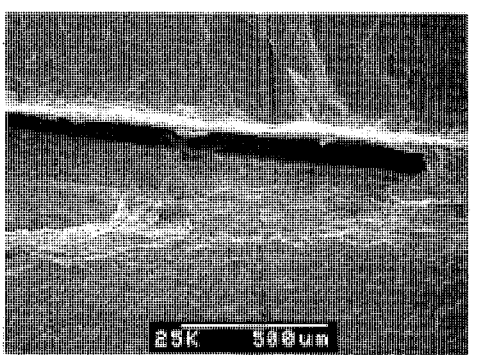

Fig.6 Fracture surface of AI-T specimen near the phase boundary.

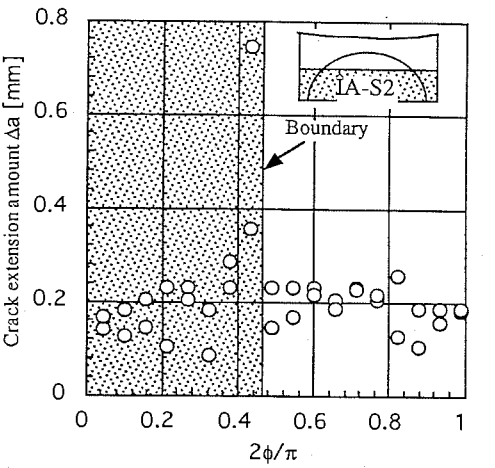

Fig.7 Stable crack growth amount △a of IA-S2 specimen along the crack front.

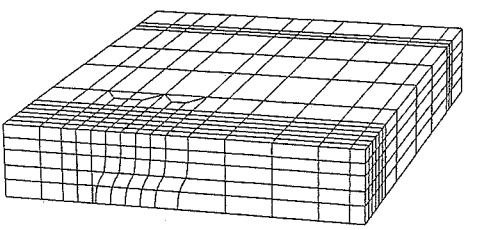

Fig.8 Mesh pattern of AI-T specimen.

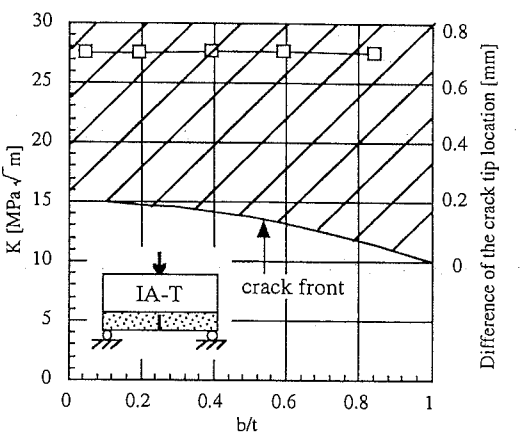

Fig.9 Results of IA-T specimen by three-dimensional elastic analysis.

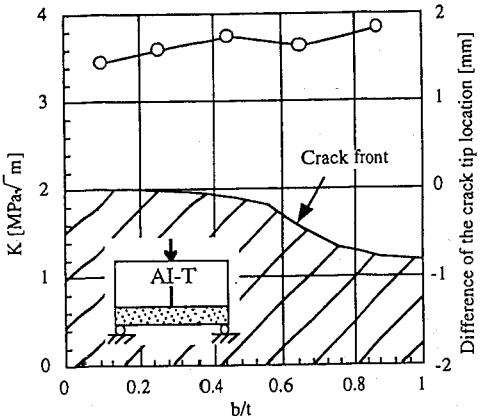

Fig. 10 Results of AI-T specimen by three-dimensional elastic analysis.

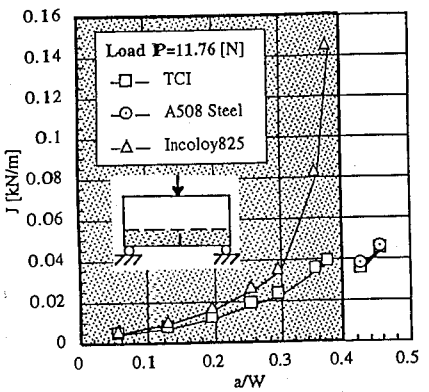

Fig. 11 Comparison of *J-a/W* relationships of TCI specimen and homogeneous materials at Load P=11.8[kN].

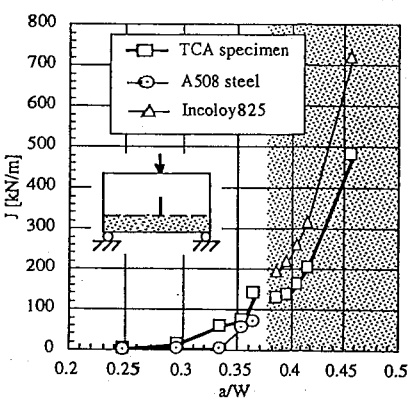

Fig. 12 Comparison of *J-a/W* relationships of TCA specimen and homogeneous materials at Load P=49[kN].

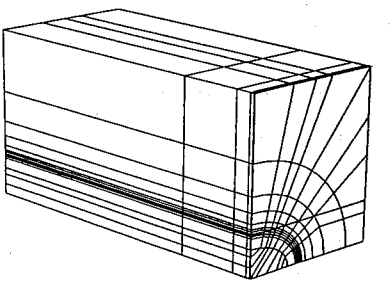

Fig. 13 Mesh pattern of IA-S1 specimen.

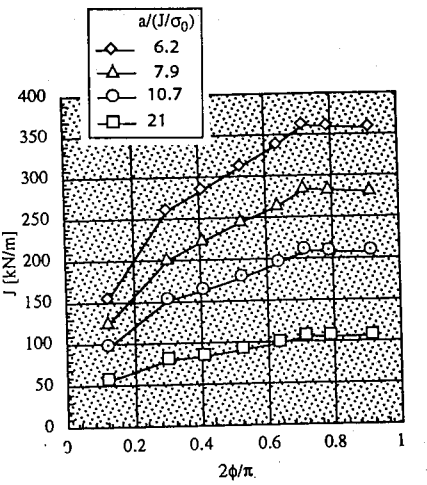

Fig. 14 J distribution along the crack front.

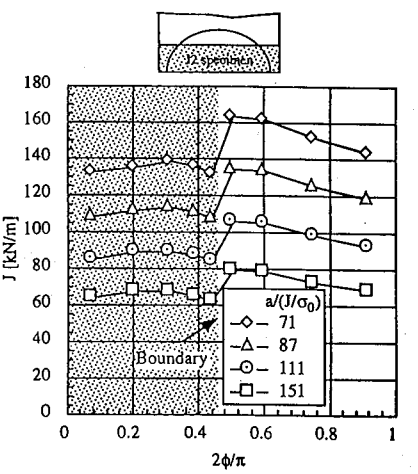

Fig. 15 *J-φ* curve of IA-S2 specimen.

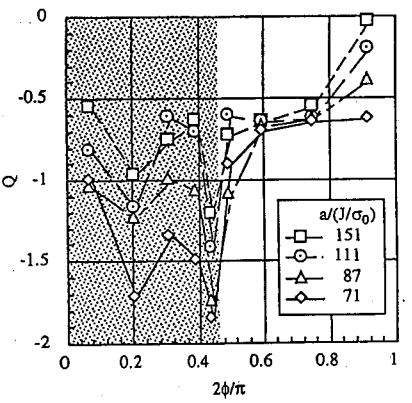

Fig.16 Distribution of Q-factor.

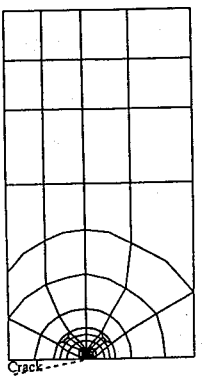

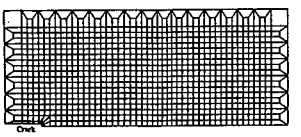

Fig.17 Mesh pattern of IA-T specimen for Modified Gurson's Model.

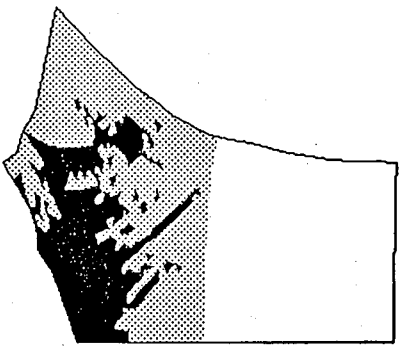

At $a/(J/\sigma_0)$=2.9 (Load P=23.6[kN])

Fig.18 Processes of fracture of TCI specimen.

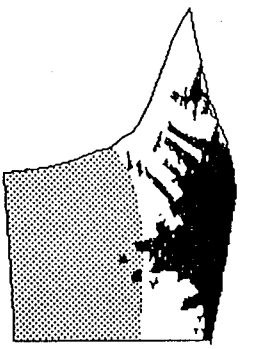

At $a/(J/\sigma_0)$=4.4 (Load P=74.6[kN])

Fig.19 Processes of fracture of TCA specimen.